DOI:
10.1109/TMI.2017.2667227

Document Version
Peer reviewed version

Distortion correction in fetal EPI using non-rigid registration with a Laplacian constraint

Maria Kuklisova-Murgasova, Georgia Lockwood Estrin, Rita G. Nunes, Shaihan J. Malik, Mary A. Rutherford, Daniel Rueckert, and Joseph V. Hajnal

***Abstract*—Geometric distortion induced by the main B0 field disrupts the consistency of fetal EPI data, on which diffusion and functional MRI is based. In this paper we present a novel data-driven method for simultaneous motion and distortion correction of fetal EPI. A motion-corrected and reconstructed T2 weighted ssFSE volume is used as a model of undistorted fetal brain anatomy. Our algorithm interleaves two registration steps: estimation of fetal motion parameters by aligning EPI slices to the model; and deformable registration of EPI slices to slices simulated from the undistorted model to estimate the distortion field. The deformable registration is regularized by a physically inspired Laplacian constraint, to model distortion induced by a source free background B0 field. Our experiments show that distortion correction significantly improves consistency of reconstructed EPI volumes with ssFSE volumes. Additionally, the estimated distortion fields are consistent with fields calculated from acquired field maps, and the Laplacian constraint is essential for estimation of plausible distortion fields. The EPI volumes reconstructed from different scans of the same subject were more consistent when the proposed method was used in comparison to EPI volumes reconstructed from data distortion corrected using a separately acquired B0 field map.**

***Index Terms*—Echo planar imaging, fetal MRI, distortion correction, B0 susceptibility induced distortion**

I. Introduction

FETAL brain magnetic resonance imaging (MRI) allows us to study the developing brain in utero. Anatomical fetal brain MRI is now well established [1]–[7], however diffusion and functional MRI, which have been widely used in adult and neonate to study microstructure and connectivity of the brain, have started emerging only recently [8]–[11]. Fetal MRI is hampered by some major technical challenges, most notably fetal motion. During acquisition the fetus is moving freely and therefore the data are acquired as stacks of 2D slices to freeze motion in time. Motion in structural fetal brain MRI has been tackled by using single shot Fast Spin Echo (ssFSE) imaging and slice-to-volume reconstruction (SVR) techniques [1]–[7]. Unlike structural imaging, functional and diffusion MRI rely on echo planar imaging (EPI) which is highly sensitive to distortion induced by static magnetic field (B0) inhomogeneity [12], [13]. An example of fetal EPI, corrupted by motion and distortion, is shown in Fig. 1. In the region of the fetal head, the distortion field is smooth and slowly varying, because the fetal head is surrounded by amniotic fluid and maternal tissue. The inhomogeneities originate from the mother's body or more focally due to gas bubbles in the gut. Such distortions disrupt the data consistency and the quality of the reconstruction. Distortions are larger at higher field, and the recent trend to move from 1.5T to 3T in fetal studies [14] makes distortion correction a timely challenge to tackle.

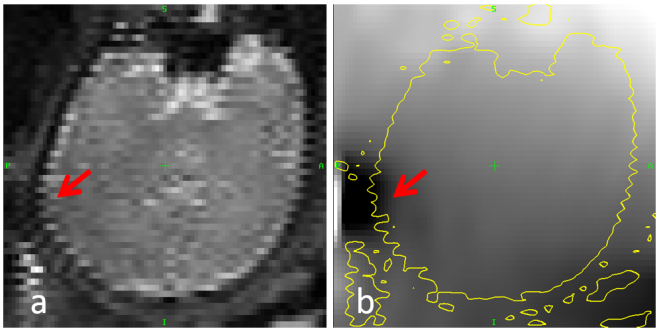

Fig. 1. Coronal view of distorted fetal brain EPI taken from axially acquired stack of slices (a) and underlying variation of B0 field (b). The red arrow points to the area of significant local distortion. Note inter-slice motion in (a), visible as a zig-zag pattern, due to slices being acquired in even and odd order.

Literature addressing the problem of B0 susceptibility induced distortion in fetal EPI is to date very limited. Wu *et al.* [15] proposed to use an acquired B0 field map [12] to correct for B0 induced distortion before SVR reconstruction. Oubel *et al.* [9] employ affine slice-to-volume registration to correct eddy current induced distortion in diffusion weighted images. Other authors do not include a distortion correction step in their methods for processing fetal EPI. On the other hand, a number of methods have been proposed to correct for spatial distortion in adult EPI [13]. A common approach is to acquire B0 field maps [12], which are typically calculated from the phase difference between two gradient echo images acquired with different echo times. This phase difference is directly proportional to spatial shifts of voxels in the phase-encoding (PE) direction of an echo planar image. Another acquisition based method is direct measurement of point spread function (PSF) of each voxel [16]. Alternatively, the distortion field can be estimated using registration-based approaches. The EPI data can be acquired with opposite phase encoding directions [17],

Maria Kuklisova-Murgasova, Shaihan J. Malik, and Joseph V. Hajnal are with Department of Biomedical Engineering, Division of Imaging Sciences, King's College London, UK

Mary A. Rutherford is with Department of Perinatal Imaging, Division of Imaging Sciences, King's College London, UK

Georgia Lockwood Estrin was with Department of Perinatal Imaging, Division of Imaging Sciences, King's College London, UK

Rita G. Nunes Instituto de Biofisica e Engenharia Biomedica, Faculdade de Ciencias, Universidade de Lisboa, Portugal and Department of Biomedical Engineering, Division of Imaging Sciences, King's College London, UK

Daniel Rueckert is with Biomedical Image Analysis Group, Imperial College London, UK

[18] and registered to find the distortion field. Alternatively, EPI can be corrected by registration to undistorted anatomical scans [19]–[21]. For correct alignment, it is important to constrain the estimated transformation [21]. B0 field inhomogeneity also causes other effects such as intensity modulation due to signal pile up or loss due to stretching. Such artefacts are often corrected by intensity modulation using the Jacobian of the displacement field [12], [19], [21], [22]. However, these tend to be small in fetal EPI, as the B0 field varies smoothly on the scale of a voxel.

In the adult case, the B0 field changes with motion, as the majority of the B0 inhomogeneity comes from air-tissue interface of the head. If only small motion is present, it can be assumed that the field map does not change, but rather it simply moves with the head [22], [23]. The acquired field map therefore needs to be aligned with the EPI prior to distortion correction, for example with a magnitude image of the field map [23], [24]. In fetal imaging there may be large amounts of motion during an examination. However, the fetal head is surrounded by water and soft tissue, and therefore the B0 inhomogeneity comes mainly from outside sources, primarily the mother's body. Consequently, fetal motion does not significantly influence the B0 field. Correction of geometric distortion in the fetus can therefore be performed using a B0 field map acquired at the beginning of the examination [15] without any need for alignment.

Accurate distortion correction is nevertheless essential in the fetal case. The large amount of motion results in slices being distorted in different directions with respect to the fetal anatomy, making the acquired data highly inconsistent. However, maternal motion during examination, such as due to respiration, or moving gas bubbles in the maternal gut, can make a pre-acquired field map become out of date, compromising distortion correction performance. We therefore proposed a novel registration-based distortion correction method for fetal EPI [25], which we present in extended form in this paper. Our method estimates the distortion directly from the acquired EPI data, making it less vulnerable to changes of the B0 field. The previous registration-based distortion correction methods for adults assumed that EPI data can be aligned to undistorted anatomical scans using volumetric registration [19]–[21] to estimate the distortion field. In the fetal case, however, we have to consider significant slice-dependent motion. Our method therefore estimates the motion parameters and the distortion field simultaneously, by registration of EPI slices to a reconstructed T2 weighted ssFSE head volume of the same subject, which is not affected by susceptibility induced distortion. The proposed registration scheme includes a physically motivated Laplacian constraint, which significantly reduces registration artifacts and thus plays a key role in estimating plausible B0 fields generated by outside sources [26]. We show that the proposed method achieves performance similar to field map correction for a set of scans selected for a good performance of the traditional field map correction.

II. Method

A. B0 field distortion in fetal EPI

The fetal head is composed of tissues of very similar magnetic susceptibility that also closely match the amniotic fluid and surrounding maternal soft tissues [27], [28]. There is no air in the frontal sinuses and the skull is not yet widely mineralised. Therefore the local B0 field variation, ΔB, is not generally changed significantly by changes of head position within womb. However, outside sources of field variation do exist and these may be in moderately close proximity to the fetal head. A common source is gas bubbles in the maternal gut. Significant distortion can therefore be present in EPI of the fetal head, but ΔB is generally smooth on the scale of individual voxels in the region of interest and since there are virtually no internal sources, ΔB obeys the Laplacian equation [26]

$$\nabla^2(\Delta B) = 0 \tag{1}$$

The EPI slices $S_t(\mathbf{y})$ are acquired as regular stacks in scanner coordinate $\mathbf{y}$, but are distorted due to ΔB. The bandwidth in the frequency encoding direction (determined from the reciprocal of the duration of an individual readout line) is typically so large that shifts and distortions in that direction are negligible. However, shifts are observable in the phase-encoding (PE) direction due to low bandwidth resulting from the duration of data acquisition being the full EPI readout. The fetal head will therefore not appear in the acquired image in location $\mathbf{y}$, but will be shifted in the PE direction by a spatially varying distance represented by a scalar field $d(\mathbf{y})$

$$d(\mathbf{y}) = \frac{\gamma \Delta B(\mathbf{y})}{bw} r_{PE} \tag{2}$$

where γ is the gyromagnetic ratio, bw is the bandwidth per pixel (determined from the reciprocal of the time taken to traverse k-space) and r_{PE} is the pixel width in the PE direction. If we denote undistorted EPI slices $S_t^u(\mathbf{y})$, then distorted and undistorted images can be related, independently of any change in fetal head position, by the following equation [12]

$$S_t(\mathbf{y} + d(\mathbf{y})\mathbf{p}) = S_t^u(\mathbf{y}) \tag{3}$$

where $\mathbf{p}$ is a unit vector along the EPI PE direction.

B. Field map based distortion correction

A field map f can be acquired as a phase difference of two gradient echo images [12]. It is directly related to B0 field variation by $f(\mathbf{y}) = \gamma \Delta B(\mathbf{y})$. Assuming that fetal motion does not cause time-dependent changes in ΔB and there is no maternal motion, ΔB can be considered fixed in scanner space and the B0 induced geometric distortions can therefore be corrected using the field map in a pre-processing step. Combining eqn. 2 and 3, we obtain

$$S_t^u(\mathbf{y}) = S_t(\mathbf{y} + f(\mathbf{y}) \frac{r_{PE}}{bw} \mathbf{p}) \tag{4}$$

C. Registration based distortion correction

As the fetus moves, the fetal head volume, $V(\mathbf{x})$, undergoes a rigid motion, represented by a rigid transformation matrix M_t, in time t, such that the anatomical location $\mathbf{x}$ in the fetal head is related to scanner coordinate $\mathbf{y}$ according to:

$$\mathbf{y} = M_t \mathbf{x} \tag{5}$$

For each time-point t we can locate the fetal head in the scanner by

$$S_t^u(\mathbf{y}) = V(M_t^{-1}\mathbf{y}) \tag{6}$$

According to eqn. 3 and 6, the acquired, distorted, EPI slice S_t can be related to the moving model of the fetal head V by:

$$S_t(\mathbf{y}_{it} + d(\mathbf{y}_{it})\mathbf{p}) = V(M_t^{-1}\mathbf{y}_{it}) \tag{7}$$

where the right side corresponds to the undistorted slice V_{M_t} simulated from the model of the fetal head volume V by sampling on the grid $\mathbf{y}_{it}$ of the acquired slice S_t. Index i defines a position of a voxel within a slice while the time-stamp t identifies the slice and is related to through-plane coordinate in the space of acquired data. The distortion field d and undistorted EPI slices S_t^u can thus be found by registration of distorted slices S_t to simulated slices V_{M_t} in the PE direction $\mathbf{p}$.

D. Model of the fetal head

Motion-corrected T2w ssFSE volumes [6] are virtually unaffected by distortions and can therefore be used as the model $V(x)$, to define the anatomical space and spatial coordinate x. Motion parameters M_t are defined relative to this anatomical space, and can be estimated by rigid registration of the distortion-corrected EPI slices to volume V. As ssFSE images do not necessarily have the same intensity ranges and contrasts as EPI data, the equality (7) does not hold, but another suitable similarity measure can be used to estimate motion and distortion. In this work we use normalized cross-correlation (NCC), because the ssFSE is largely T2 weighted and the EPI is T2 and/or T2* weighted. Thus the motion and distortion can be estimated by optimizing the following objective function over distortion field d and motion parameters M

$$\begin{aligned} F(d,M) &= NCC(S_d, V_M) \\ &= \frac{\sum_{it}(S_d(\mathbf{y}_{it}) - \bar{S}_d)(V_M(\mathbf{y}_{it}) - \bar{V}_M)}{\sqrt{\sum_{it}(S_d(\mathbf{y}_{it}) - \bar{S}_d)^2 \sum_{it}(V_M(\mathbf{y}_{it}) - \bar{V}_M)^2}} \end{aligned}$$

where S_d and V_M denote the stacks of distortion-corrected and simulated slices respectively, defined as $S_d(\mathbf{y}_{it}) = S_t(\mathbf{y}_{it} + d(\mathbf{y}_{it})\mathbf{p})$ and $V_M(\mathbf{y}_{it}) = V(M_t^{-1}\mathbf{y}_{it}))$. Additionally, $\bar{S}_d$ and $\bar{V}_M$ denote means of image intensities in S_d and V_M, respectively.

E. Laplacian constraint

The estimated distortion field d should obey Laplace's equation (1) in the region of the fetal head. We therefore amend the objective function by introducing a regularisation term

$$L(d) = \frac{1}{R}\iiint_R \left(\frac{\partial^2 d}{\partial u^2} + \frac{\partial^2 d}{\partial v^2} + \frac{\partial^2 d}{\partial w^2}\right)^2 du\, dv\, dw$$

where R is the region of interest in scanner space covering the fetal head but excluding any sources of B0 field inhomogeneity, and u, v, w are the 3D coordinates in the scanner space. This regularisation term is in the form of L2 norm of Laplacians of the distortion field d and thus penalises deviations from Laplace's equation (1). The Laplacian constraint also helps to prevent unrealistic deformations resulting from the differences in ssFSE and EPI contrasts.

The final regularized objective function F_R to be optimized for the estimation of d and M_t can thus be written as

$$F_R(d,M) = F(d,M) - \lambda L(d) \tag{8}$$

where the parameter λ represents the trade-off between the data term F and the regularization constraint L.

III. Implementation

Optimisation of the objective function (8) consists of two steps: rigid registration of the acquired EPI slices S_t to the model V to estimate motion parameters M_t; and deformable registration of acquired EPI slices S_t to simulated slices V_{M_t} in PE direction only, regularized by the Laplacian constraint, to estimate a smooth distortion field d. These are performed in an iterative manner, and as the iterations progress, motion parameters can be adjusted by registering distortion-corrected rather than original acquired EPI slices.

The registration is performed using the IRTK software package [29]. The motion parameters are estimated by rigid registration and distortion by B-spline registration [30] with normalized cross-correlation (NCC) as a similarity measure. We have chosen a relatively large control point spacing 10mm for B-spline transformation, as this helps to prevent large unrealistic deformations while being sufficient to describe smooth distortion fields. The Laplacian regularisation is incorporated within the B-spline registration and is evaluated analytically on the same grid as B-spline control points for computational efficiency.

We run the algorithm for four iterations while progressively increasing the number of free motion parameters as follows: In iteration 1 we perform volumetric registration of EPI stacks to a previously motion corrected and reconstructed ssFSE volume, in iteration 2 each EPI stack is split in even and odd slices (this is consistent with the slice acquisition order) and in iteration 3 and 4 each EPI slice is individually aligned with the ssFSE volume using its own rigid transformation. Using a small number of iterations is important because adding extra iterations is time consuming. The distortion is re-estimated during each iteration. Finally an EPI volume is reconstructed at the end of the process using our previously proposed method [6]. The algorithm is illustrated in Fig. 2.

The parallel CPU implementation of this algorithm was run on personal PC with 12 core CPU. The running times were between 5 and 30 minutes depending on the size of the fetal head.

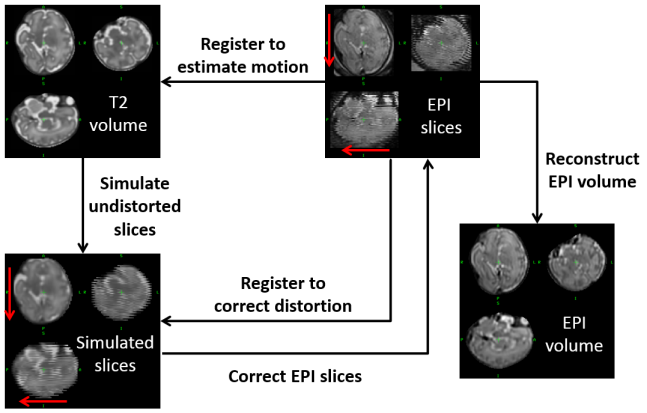

Fig. 2. Summary of the proposed algorithm.

IV. Experiments

The proposed distortion correction and reconstruction method was applied to 15 EPI scans of the fetal head for 7 different subjects, each consisting of four stacks of slices acquired on the same grid. The acquisition consisted of the scans acquired in the following order: First B0 field map, first transverse b=0 scan, diffusion weighted scan (b=500smm^{-2}, 15 directions), second transverse b=0 scan, coronal b=0 scan, second B0 field map. The experiments in this paper were performed using b=0 scans and B0 field maps only. In three cases the coronal scan was missing due to lack of scanning time. One transverse scan was excluded due to motion being too large to be corrected using our slice-to-volume registration. Additionally distortion correction using the B0 field maps directly was performed for all the scans and visually assessed by comparison with reconstructed ssFSE data. Two coronal scans were excluded because of failed field map correction.

Images were acquired using a spin-echo diffusion sequence, with diffusion gradients set to zero (dMRI b=0smm^{-2}, TE 121ms, TR 8500ms, FoV 290x290x128mm^3, voxel size 2.3x2.3x3.5mm^3, slice overlap 1.75mm). T2 weighted volumes reconstructed using our previously proposed method [6] from ssFSE slices (a total 8 stacks of slices, acquired in a mix of three orthogonal directions, TR 15000ms, TE 180ms, excitation flip angle 90^o, refocusing flip angle 160^o, half Fourier factor 0.63, FoV 290x290x128mm^3, voxel size 1.25x1.25x2.5mm^3, slice overlap 1.25mm) and acquired B0 field maps (TE1 4.6ms, TE2 9.2ms; TR 10ms, Flip Angle 10^o, voxel size 2.27x2.27x10mm^3, FoV 400x400x150mm^3) were available for all the scans.

A. Experiment with fixed motion parameters

In the first experiment (Section V-A) we evaluated performance of the distortion correction element of the proposed method by comparing the estimated distortion field to the distortion field calculated from the acquired field maps (eqn. 2). It should be noted that there is not a unique solution for optimal motion and distortion parameters: translation of the slices in the PE direction can be interpreted either as a motion or a distortion. The algorithm is thus capable of correctly estimating the undistorted slices, but not necessarily the true motion and distortion parameters. We therefore estimated the motion parameters M_t ahead of the registration-based distortion correction by aligning field map corrected EPI slices to the ssFSE T2w volume V. The distortion field was then estimated using the fixed motion parameters as follows: Simulated slices V_M were calculated using the fixed motion parameters. The distortion field d was obtained by registration of acquired distorted slices S_t to simulated undistorted slices V_{M_t} by maximizing the objective function (8). The objective function (8) was optimized for several values of parameter λ. The estimated distortion fields were compared to the distortion fields calculated from acquired field maps, which served as the "ground truth" for this experiment, by calculating the root mean squared error (RMSE) between them, evaluated pointwise over the fetal brain:

$$RMSE(d, d_a) = \sqrt{\frac{\sum_{iz}(d(\mathbf{y}_{iz}) - d_a(\mathbf{y}_{iz}))^2}{n}} \qquad (9)$$

where d is the estimated distortion field, d_a is the distortion field calculated from acquired field map (eqn. 2), and y_{iz} is the voxel grid in the acquired image space.

B. Evaluation of the convergence of the proposed method

In Sec. V-B we investigate convergence properties of the the full algorithm with interleaved estimation of motion M_t and distortion d. We first evaluate the objective function (8) to demonstrate the convergence of the algorithm. For one of the scans we evaluated the objective function for 20 iterations. We performed independent slice-to-volume registration interleaved with distortion correction for the last 18 rather than just last the two iterations. Additionally we evaluated the objective function for each of the four iterations described in Sec. III for all the scans.

C. Consistency of ssFSE and EPI volumes

To further evaluate the convergence properties of the proposed method we calculate consistency of reconstructed EPI volumes with the ssFSE T2w volume of the same subject quantified using NCC as a similarity metric, which we present is Sec. V-C. As described in Section IV, one of the selection criteria for this data set was that field map distortion correction produces visually plausible results. We therefore use the consistency of the field map and motion corrected EPI volume with ssFSE volume as a benchmark for a good performance of the proposed method.

To perform this comparison we reconstructed EPI volumes using three different methods: 1. Uncorrected EPI slices S_t were registered to ssFSE volume V to estimate parameters M_t, followed by super-resolution reconstruction with outlier rejection [6] (no correction); 2. EPI slices S_{d_a} corrected by an acquired field map were registered to ssFSE volume V to estimate parameters M_t, followed by super-resolution reconstruction with outlier rejection [6] (field map); 3. Interleaved motion and distortion correction to estimate motion parameters M_t, distortion d and undistorted slices S_d by registration to ssFSE volume V, followed by super-resolution reconstruction with outlier rejection [6] (proposed).

D. Comparison of EPI volumes

In section V-D we evaluate consistency of EPI volumes of the same subjects reconstructed from different scans with no distortion correction, field map correction and the proposed method, as described in sec. IV-C. First we compare EPI volumes reconstructed from transverse and coronal stacks acquired very close in time but with orthogonal phase encoding directions. These scans have a single acquired field map associated with them. Such scans were available for two subjects. In the second experiment we compare EPI volumes reconstructed from transverse EPI scans that were acquired at different times (e.g. before and after a full 15 direction diffusion scan) and which have different field maps associated with them. Such scans were available for six subjects.

V. Results

A. Comparison with acquired field maps

The experiment with fixed motion parameters (Sec. IV-A) was performed on all 15 EPI scans consisting of 4 stacks of slices of the same orientation acquired on the same grid. The distortion field estimation was performed using following values for the parameter $\lambda = 0, 0.0001, 0.001, 0.01, 0.1, 0.5, 0.8, 1$. The RMSE between estimated distortion fields and distortion fields calculated from acquired field maps that was averaged over all voxels in region of interest and all scans, is presented in Fig. 3 and Table I. We can observe that the average error for non-regularized B-spline registration is 0.76mm. This value drops to 0.5mm for $\lambda = 0.5$.

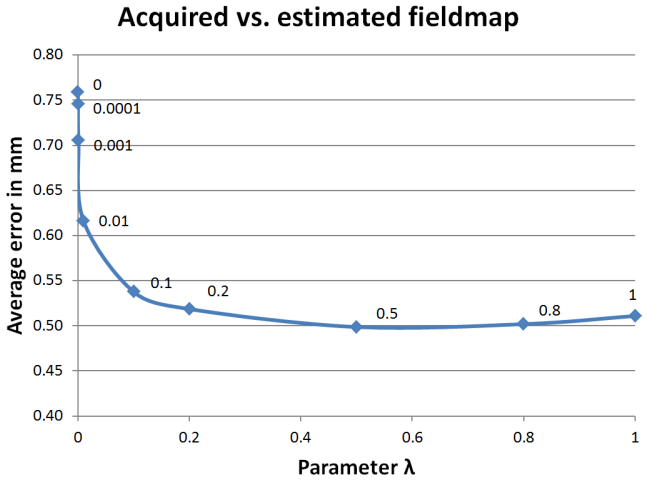

Fig. 3. RMSE between estimated distortion fields and distortion fields calculated from acquired field maps for different values of λ parameter.

Visualisation of influence of the parameter λ on the estimated distortion field is presented in Fig. 4. When no Laplacian regularisation is used ($\lambda = 0$), there are deformations within the region of interest that violate Laplace's equation, making the distortion field not smooth and unphysical for a region approximately free of sources of B0 inhomogeneity. As λ increases, the distortion field becomes smoother. After $\lambda = 0.1$ no further improvement in smoothness of the distortion field is seen, however, the significant local B0 variation that appears dark starts fading. When values larger than $\lambda = 0.1$ are used, the proposed method loses capability to correct for significant local distortion (compare to distortion field calculated from acquired field map in bottom right corner of Fig. 4). Visual inspection suggests that even though the field maps are closest to acquired field maps for $\lambda = 0.5$ on average, this value might be too high when significant local distortion is present. We therefore selected $\lambda = 0.1$ for further experiments. In Fig. 5 we present examples of distortion correction of EPI data using the chosen value.

B. Evaluation of the convergence of the proposed method

The evaluation of the objective function (8) for 20 iterations for Subject 1 presented in Fig. 6 shows that the objective function value stabilises after four iterations. Additionally we also found that the value of the objective function increased at each of the four iterations for all scans. Average values of objective function over all scans are presented at Table II.

C. Consistency of ssFSE and EPI volumes

The NCC measuring consistency of ssFSE and EPI volumes, as described in Section IV-C are presented in Table III. We can observe that distortion correction with either the acquired field map (field map) or the proposed method (proposed) results in improved consistency with ssFSE volumes in all cases compared to when no distortion correction was performed (no correction). It can be seen in Table III that consistency for the proposed method is higher than for the field map for all subjects.

D. Comparison of EPI volumes

In this section we present comparison of the EPI volumes of the same subject reconstructed from different scans. Tables IV and V show consistency of volumes reconstructed form transverse and coronal stacks, and transverse stacks acquired at different times, respectively. We compared consistency for the three reconstruction methods described in Section IV-D. We can conclude that distortion correction using either a B0 field map or the proposed method improves the consistency, while consistency of volumes reconstructed using the proposed method results in the highest NCC in all cases.

VI. Discussion

The registration-based distortion correction method for fetal EPI presented in this paper was compared to field map based distortion correction. For this purpose we chose datasets where a field map was available and sufficiently accurate, as explained in Section IV. Under this scenario we showed a good consistency of estimated and acquired field maps (sec. V-A). Additionally, we showed that there was small improvement in consistency of reconstructed EPI volumes from different scans of the same subject when the registration-based method was used, as opposed to the field map correction. However, the main application of the registration-based method is in cases when the acquired field map is not available, or the

TABLE I
RMSE BETWEEN ACQUIRED AND ESTIMATED FIELD MAPS FOR DIFFERENT VALUES OF λ PARAMETER.

Lambda	0	0.0001	0.001	0.01	0.1	0.2	0.5	0.8	1
Average error (mm)	0.76	0.75	0.71	0.62	0.54	0.52	0.50	0.50	0.51
Stdev (mm)	0.18	0.18	0.17	0.16	0.16	0.15	0.15	0.150	0.15

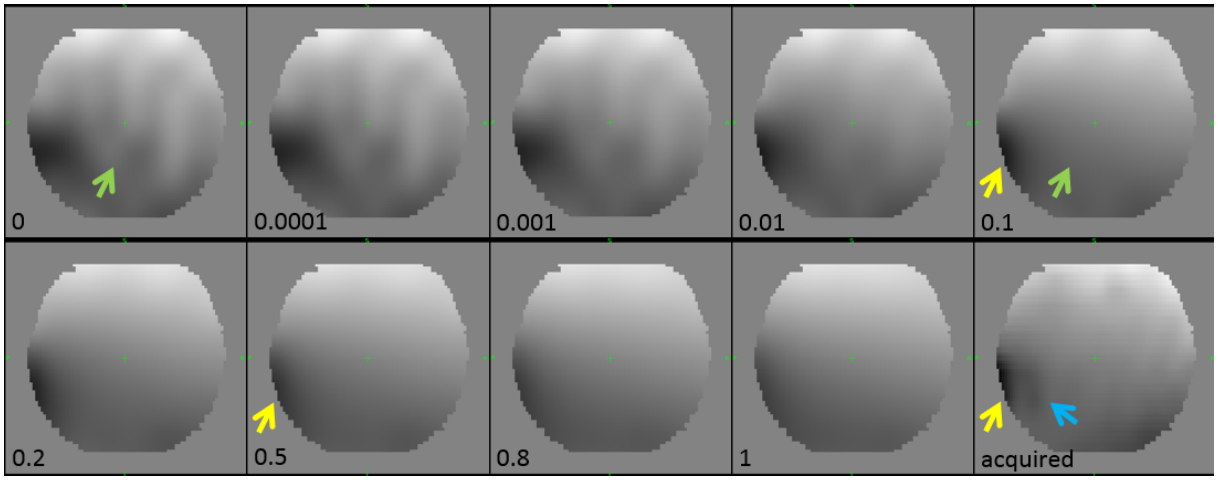

Fig. 4. Comparison estimated distortion fields with various values of parameter λ and the distortion field calculated from the acquired field map. Yellow arrows point to the area of local distortion which is consistent with the acquired field map for $\lambda = 0.1$, but starts fading for $\lambda = 0.5$. Green arrows point to artefact present if Laplacian constraint is not used and not present for $\lambda = 0.1$. Blue arrow points to acquisition artefacts in the acquired field map.

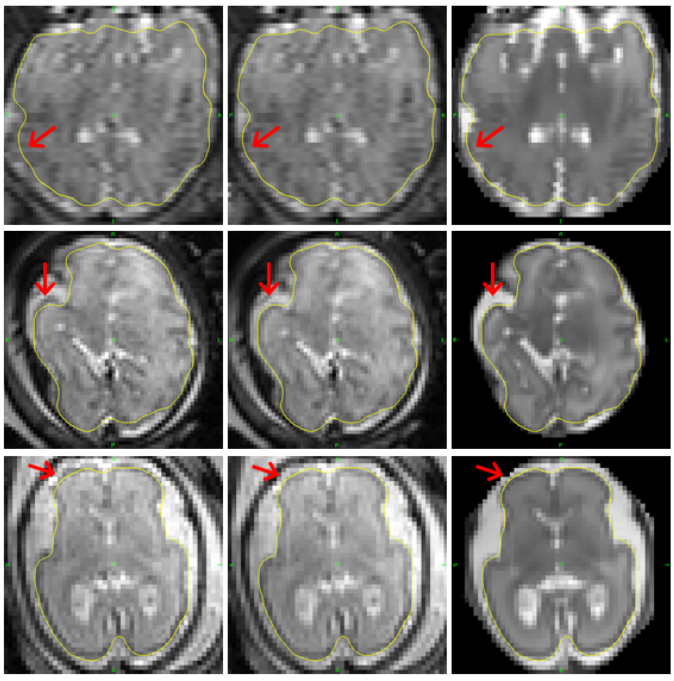

Fig. 5. Comparison of original distorted stacks and stacks corrected using the proposed method with fixed motion parameters. First column: acquired stacks. Second column: corrected stacks. Third column: corresponding stacks simulated from ssFSE volume. Rows correspond to three different subjects acquired in approximately transverse orientation. The first row shows a coronal cut through the stack of transverse slices, the other two show a single transverse slice. Please note that the data are presented in the orientation of acquisition. Red arrows highlight distortions in original acquired slices (left column), identified by comparison to slices simulated from ssFSE volume (right column), as highlighted by yellow outlines. In the corrected stacks these distortions are not present (middle column).

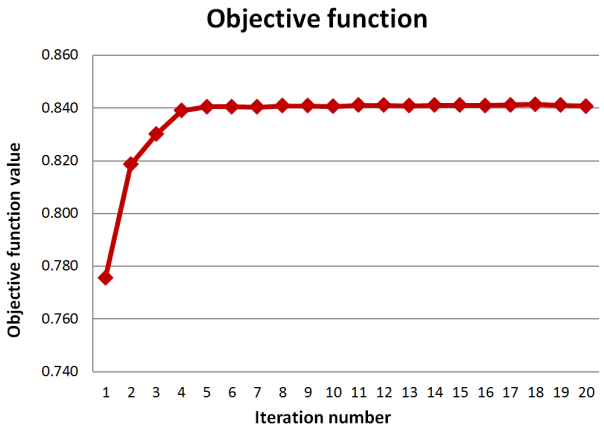

Fig. 6. Evaluated objective function for 20 iterations of the proposed method for Subject 1.

TABLE II
AVERAGE VALUE OF OBJECTIVE FUNCTION AT EACH OF THE FOUR ITERATIONS CALCULATED OVER ALL 15 SCANS.

Iteration	1	2	3	4
Average objective function value	0.63	0.70	0.73	0.75

assumptions for its use are violated. In our experience, the performance of field map based distortion correction in fetus can vary from case to case, depending on amount of maternal motion between acquisition of field map and EPI data, or human errors that occur during acquisition or recording. In

TABLE III
CONSISTENCY OF RECONSTRUCTED EPI VOLUMES WITH SSFSE T2 VOLUMES OF THE SAME SUBJECT MEASURED USING NCC, WITHOUT DISTORTION CORRECTION, AND WITH DISTORTION CORRECTION USING EITHER THE ACQUIRED B0 FIELD MAP OR THE PROPOSED METHOD. THE HIGHEST CONSISTENCY IS HIGHLIGHTED IN BOLD (PLEASE NOTE DIFFERENCES MIGHT NOT ALWAYS BE VISIBLE DUE TO ROUNDING TO 2 DECIMAL PLACES)

Subject	scan	no correction	field map	proposed
Subj 1	transverse 1	0.76	0.77	**0.79**
Subj 1	transverse 2	0.73	0.77	**0.79**
Subj 1	coronal	0.73	0.76	**0.78**
Subj 2	transverse 1	0.66	0.68	**0.69**
Subj 2	transverse 2	0.64	0.67	**0.69**
Subj 3	transverse 2	0.63	0.68	**0.70**
Subj 3	coronal	0.58	0.70	**0.74**
Subj 4	transverse 1	0.72	0.75	**0.77**
Subj 4	transverse 2	0.71	0.75	**0.79**
Subj 5	transverse 1	0.65	0.68	**0.68**
Subj 5	transverse 2	0.63	0.69	**0.70**
Subj 6	transverse 1	0.69	0.76	**0.78**
Subj 6	transverse 2	0.70	0.76	**0.78**
Subj 7	transverse 1	0.72	0.78	**0.79**
Subj 7	transverse 2	0.73	0.77	**0.78**
average		0.68±0.05	0.73±0.04	**0.75±0.05**

TABLE IV
COMPARISON OF RECONSTRUCTED CORONAL AND TRANSVERSE EPI IMAGES USING NCC, WITHOUT DISTORTION CORRECTION, AND WITH DISTORTION CORRECTION USING EITHER ACQUIRED B0 FIELD MAP OR THE PROPOSED METHOD.

	No correction	field map	proposed
Subj 1	0.77	0.84	**0.89**
Subj 3	0.68	0.81	**0.85**

these cases the performance of correction using the acquired field map can drop sharply, while the proposed alternative approach could still recover the original undistorted anatomy of the fetal brain.

In Fig. 7 we show a transverse view of a field map acquired at the beginning and end of the examination. We can clearly see that the field map has changed in time, in this case due to a gas bubble moving in the maternal gut. This example demonstrates that B0 field does vary in time, which is one of the main reasons why estimating the distortion from the data can be more successful, than acquiring the field map beforehand. Note also that the acquired field map shows some signs of local maxima and minima (see Fig. 4 and 7). This is probably caused by acquisition artefacts, which would imply that acquired field maps are not necessarily completely accurate and differences between acquired and estimated field maps can be caused by errors in both.

In this paper we proposed a method for estimation of distortion field from b=0 dMRI. However in practice distortion correction needs to be applied to diffusion weighted scans as well to allow further processing and analysis. In the current framework the distortion field can be estimated from the b=0 scans and subsequently applied to diffusion weighted scans. We show an example in Fig. 8. However, this does not allow correcting the distortion in presence of changing B0 field. This issue can be addressed by amending the scanning protocol to interleave acquisition of b=0 and diffusion weighted data. This way diffusion weighted scans can be corrected using field maps estimated from temporally adjacent b=0 images.

TABLE V
COMPARISON OF RECONSTRUCTED TRANSVERSE EPI IMAGES ACQUIRED AT DIFFERENT TIMES USING LOCAL NCC, WITHOUT DISTORTION CORRECTION, AND WITH DISTORTION CORRECTION USING EITHER ACQUIRED B0 FIELD MAP OR THE PROPOSED METHOD.THE BEST VALUES ARE HIGHLIGHTED IN BOLD (PLEASE NOTE DIFFERENCE MIGHT NOT ALWAYS BE VISIBLE DUE TO ROUNDING).

	No correction	field map	proposed
Subj 1	0.95	0.97	**0.98**
Subj 2	0.93	0.93	**0.94**
Subj 4	0.89	0.91	**0.93**
Subj 5	0.88	0.89	**0.91**
Subj 6	0.94	0.95	**0.95**
Subj 7	0.92	0.93	**0.94**

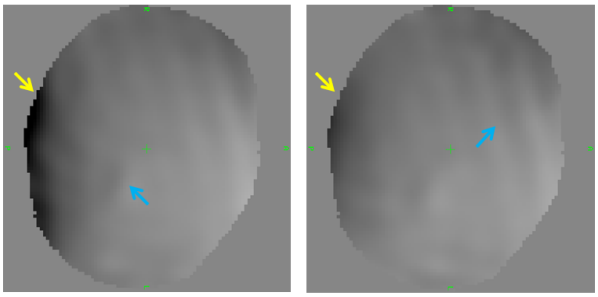

Fig. 7. Change in acquired field map at the beginning and the end of the examination. Yellow arrows point to the area of the visible difference. Blue arrows highlight the acquisition artefacts in the field maps.

VII. CONCLUSION

In this paper we presented a method for distortion correction of fetal EPI based on registration to undistorted reconstructed ssFSE volumes of the same subject using a physically inspired regularisation term. We demonstrated the importance of applying distortion correction to fetal EPI data. Our results show that the proposed method provides a viable alternative to correction using acquired B0 field maps, which is especially important in cases when acquired field maps are not available, or the field map based distortion correction is disrupted by maternal motion or human error.

ACKNOWLEDGMENT

This work has been supported by MRC strategic grant MR/K006355/1. RGN was funded by the Portuguese Foundation for Science and Technology grants UID/BIO/00645/2013 and IF/00364/2013.

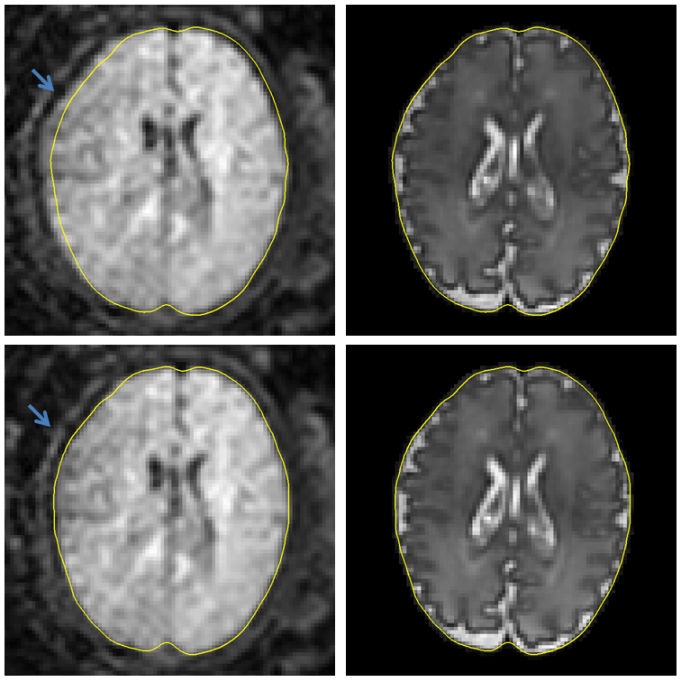

Fig. 8. Impact of distortion correction on diffusion weighted data. Top left: distorted diffusion weighted slice. Top right: corresponding cut through the reconstructed ssFSE volume aligned with distorted diffusion weighted slice. Bottom left: diffusion weighted slice corrected using the distortion field calculated using the proposed method from corresponding b=0 scans. Bottom right: corresponding cut through the reconstructed ssFSE volume aligned with corrected diffusion weighted slice. Yellow contours show the brain outline in ssFSE volume. Blue arrow points to area of visible distortion in the diffusion weighted slice successfully corrected using the proposed method.

REFERENCES

[1] F. Rousseau, O. A. Glenn, B. Iordanova, C. Rodriguez-Carranza, D. B. Vigneron, J. A. Barkovich, and C. Studholme, "Registration-based approach for reconstruction of high-resolution in utero fetal MR brain images," *Academic Radiology*, vol. 13, no. 9, pp. 1072 – 1081, 2006.

[2] S. Jiang, H. Xue, A. Glover, M. Rutherford, D. Rueckert, and J. Hajnal, "MRI of moving subjects using multislice snapshot images with volume reconstruction (SVR): Application to fetal, neonatal, and adult brain studies," *IEEE Transactions on Medical Imaging*, vol. 26, no. 7, pp. 967 –980, July 2007.

[3] K. Kim, P. Habas, F. Rousseau, O. Glenn, A. Barkovich, and C. Studholme, "Intersection based motion correction of multislice MRI for 3-D in utero fetal brain image formation," *IEEE Transactions on Medical Imaging*, vol. 29, no. 1, pp. 146 –158, Jan. 2010.

[4] F. Rousseau, K. Kim, C. Studholme, M. Koob, and J.-L. Dietemann, "On super-resolution for fetal brain MRI," in *Medical Image Computing and Computer Assisted Intervention*, 2010.

[5] A. Gholipour, J. Estroff, and S. Warfield, "Robust super-resolution volume reconstruction from slice acquisitions: Application to fetal brain MRI," *IEEE Transactions on Medical Imaging*, vol. 29, no. 10, pp. 1739 –1758, 2010.

[6] M. Kuklisova-Murgasova, G. Quaghebeur, M. A. Rutherford, J. V. Hajnal, and J. A. Schnabel, "Reconstruction of fetal brain MRI with intensity matching and complete outlier removal," *Medical Image Analysis*, vol. 16, no. 8, pp. 1550 – 1564, 2012.

[7] S. Tourbier, X. Bresson, P. Hagmann, J.-P. Thiran, R. Meuli, and M. B. Cuadra, "An efficient total variation algorithm for super-resolution in fetal brain {MRI} with adaptive regularization," *NeuroImage*, vol. 118, pp. 584 – 597, 2015.

[8] S. Jiang, H. Xue, S. Counsell, M. Anjari, J. Allsop, M. Rutherford, D. Rueckert, and J. V. Hajnal, "Diffusion tensor imaging (DTI) of the brain in moving subjects: Application to in-utero fetal and ex-utero studies," *Magnetic Resonance in Medicine*, vol. 62, no. 3, pp. 645–655, 2009.

[9] E. Oubel, M. Koob, C. Studholme, J.-L. Dietemann, and F. Rousseau, "Reconstruction of scattered data in fetal diffusion MRI," *Medical Image Analysis*, vol. 16, no. 1, pp. 28 – 37, 2012.

[10] M. Fogtmann, S. Seshamani, C. Kroenke, X. Cheng, T. Chapman, J. Wilm, F. Rousseau, and C. Studholme, "A unified approach to diffusion direction sensitive slice registration and 3-D DTI reconstruction from moving fetal brain anatomy," *Medical Imaging, IEEE Transactions on*, vol. 33, no. 2, pp. 272–289, 2014.

[11] G. Ferrazzi, M. K. Murgasova, T. Arichi, C. Malamateniou, M. J. Fox, A. Makropoulos, J. Allsop, M. Rutherford, S. Malik, P. Aljabar, and J. V. Hajnal, "Resting state fMRI in the moving fetus: A robust framework for motion, bias field and spin history correction," *NeuroImage*, vol. 101, pp. 555 – 568, 2014.

[12] P. Jezzard and R. S. Balaban, "Correction for geometric distortion in echo planar images from B0 field variations," *Magnetic Resonance in Medicine*, vol. 34, no. 1, pp. 65–73, 1995.

[13] P. Jezzard, "Correction of geometric distortion in fMRI data," *NeuroImage*, vol. 62, no. 2, pp. 648 – 651, 2012.

[14] T. Victoria, D. Jaramillo, T. P. L. Roberts, D. Zarnow, A. M. Johnson, J. Delgado, E. Rubesova, and A. Vossough, "Fetal magnetic resonance imaging: jumping from 1.5 to 3 tesla (preliminary experience)," *Pediatric Radiology*, vol. 44, no. 4, pp. 376–386, 2014.

[15] Z. Wu, R. G. Nunes, S. J. Malik, G. L. Estrin, E. J. Hughes, C. Malamateniou, S. J. Counsell, M. A. Rutherford, and J. V. Hajnal, "Fetal imaging with EPI - FOV, SNR and distortion correction," in *International Society for Magnetic Resonance Imaging*, 2012.

[16] M. D. Robson, J. Gore, and R. T. Constable, "Measurement of the point spread function in MRI using constant time imaging," *Magnetic resonance in medicine*, vol. 38, no. 5, pp. 733–740, 1997.

[17] J. L. Andersson, S. Skare, and J. Ashburner, "How to correct susceptibility distortions in spin-echo echo-planar images: application to diffusion tensor imaging," *NeuroImage*, vol. 20, no. 2, pp. 870 – 888, 2003.

[18] "Efficient correction of inhomogeneous static magnetic field-induced distortion in echo planar imaging," *NeuroImage*, vol. 50, no. 1, pp. 175 – 183, 2010.

[19] C. Studholme, R. T. Constable, and J. S. Duncan, "Accurate alignment of functional EPI data to anatomical MRI using a physics-based distortion model," *IEEE Transactions on Medical Imaging*, vol. 19, no. 11, pp. 1115–1127, 2000.

[20] J. Kybic, P. Thevenaz, A. Nirkko, and M. Unser, "Unwarping of unidirectionally distorted EPI images," *IEEE Transactions on Medical Imaging*, vol. 19, no. 2, pp. 80–93, 2000.

[21] A. Gholipour, N. Kehtarnavaz, K. Gopinath, and R. Briggs, "Cross-validation of deformable registration with field maps in functional magnetic resonance brain imaging," *IEEE Journal of Selected Topics in Signal Processing*, vol. 2, no. 6, pp. 854–869, 2008.

[22] J. L. Andersson and S. N. Sotiropoulos, "An integrated approach to correction for off-resonance effects and subject movement in diffusion MR imaging," *NeuroImage*, vol. 125, pp. 1063 – 1078, 2016.

[23] "FSL," *NeuroImage*, vol. 62, no. 2, pp. 782 – 790, 2012.

[24] R. Cusack, M. Brett, and K. Osswald, "An evaluation of the use of magnetic field maps to undistort echo-planar images," *NeuroImage*, vol. 18, no. 1, pp. 127 – 142, 2003.

[25] M. K. Murgasova, G. L. Estrin, M. Rutherford, D. Rueckert, and J. Hajnal, "Distortion correction in fetal EPI using non-rigid registration with Laplacian constraint," in *2016 IEEE 13th International Symposium on Biomedical Imaging (ISBI)*, 2016, pp. 1372–1375.

[26] F. Schweser, A. Deistung, B. W. Lehr, and J. R. Reichenbach, "Quantitative imaging of intrinsic magnetic tissue properties using MRI signal phase: An approach to in vivo brain iron metabolism?" *NeuroImage*, vol. 54, no. 4, pp. 2789 – 2807, 2011.

[27] C. Poynton, M. Jenkinson, and W. Wells, "Atlas-based improved prediction of magnetic field inhomogeneity for distortion correction of EPI data." in *Medical image computing and computer-assisted intervention(MICCAI 2009)*, 2016, pp. 951–959.

[28] W. Li, B. Wu, A. Batrachenko, V. Bancroft-Wu, R. A. Morey, V. Shashi, C. Langkammer, M. D. De Bellis, S. Ropele, A. W. Song, and C. Liu, "Differential developmental trajectories of magnetic susceptibility in human brain gray and white matter over the lifespan," *Human Brain Mapping*, vol. 35, no. 6, pp. 2698–2713, 2014.

[29] "IRTK - Image Registration Toolkit," https://biomedia.doc.ic.ac.uk/software/irtk.

[30] D. Rueckert, L. Sonoda, C. Hayes, D. Hill, M. Leach, and D. Hawkes, "Nonrigid registration using free-form deformations: application to breast MR images," *Medical Imaging, IEEE Transactions on*, vol. 18, no. 8, pp. 712–721, 1999.